

Noise is an Efficient Learner for Zero-Shot Vision-Language Models

Raza Imam Asif Hanif Jian Zhang Khaled Waleed Dawoud
 Yova Kementchedjhieva Mohammad Yaqub
 Mohamed bin Zayed University of Artificial Intelligence (MBZUAI), UAE
 {firstname.lastname}@mbzuai.ac.ae
<https://github.com/Razaimam45/TNT>

Abstract

Recently, test-time adaptation has garnered attention as a method for tuning models without labeled data. The conventional *modus operandi* for adapting pre-trained vision-language models (VLMs) during test-time primarily focuses on tuning learnable prompts; however, this approach overlooks potential distribution shifts in the visual representations themselves. In this work, we address this limitation by introducing **Test-Time Noise Tuning (TNT)**, a novel method for handling unpredictable shifts in the visual space. TNT leverages, for the first time, a **noise adaptation** strategy that optimizes learnable noise directly in the visual input space, enabling adaptive feature learning from a single test sample. We further introduce a novel approach for inter-view representation alignment by explicitly enforcing coherence in embedding distances, ensuring consistent feature representations across views. Combined with scaled logits and confident view selection at inference, TNT substantially enhances VLM generalization and calibration, achieving average gains of +7.38% on natural distributions benchmark and +0.80% on cross-dataset evaluations over zero-shot CLIP. These improvements lay a strong foundation for adaptive out-of-distribution handling.

1. Introduction

Vision-language models (VLMs) have been shown to successfully perform various downstream tasks in a zero-shot fashion, which eliminates the need for creating task-specific training data and storing multiple models. The ability of VLMs to generalize on open-world problems, however, degrades as real-world data shifts away from the distribution that the models were trained on. Test-Time Adaptation (TTA) has thus emerged as a critical approach to enhance model robustness while maintaining the advantages of zero-shot learning [30, 32]. TTA operates at inference time, leveraging unlabeled test data to dynamically adjust existing or newly added model parameters to the desired

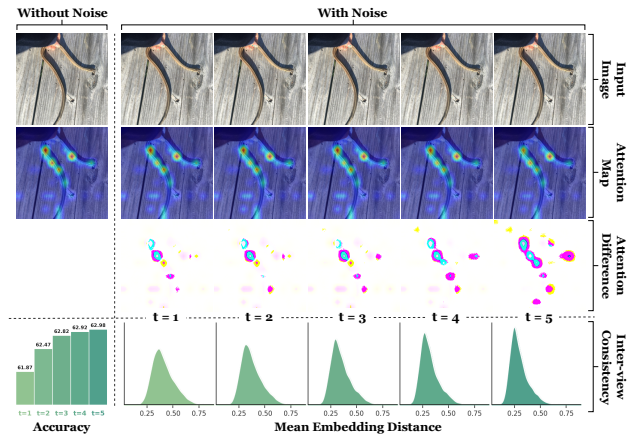


Figure 1. As top- K augmented view embeddings grow more consistent with each optimization step t , the attention mechanism focuses on relevant regions, leading to improved accuracy. *Attention Difference* illustrates the absolute difference between the clean attention map and the noise-tuned attention map. CLIP zero-shot incorrectly classifies the original image as **amaga**, while TNT correctly classifies the optimized image as **garter snake**.

distribution.

Various forms of parametrization for TTA have been explored, both on the side of the image encoder and the text encoder of VLMs [35]. These include learning a soft prompt for the text encoder [20, 27, 36], adapting the batch norm layers of the VLM [18, 38], learning LoRA layers in model components [14], or even updating whole components of the model, such as the vision encoder [40]. Amidst an abundance of TTA studies, one form of parametrization that remains unexplored is *noise*.

While noise is often seen as disruptive to machine learning models, it has also proved valuable in many ways. In generative models such as generative adversarial networks [6], variational autoencoders [16], and, more recently, diffusion models [13, 23, 26], *random* noise has been used to initialize and guide output generation with impressive results. Building on findings that noise can enhance represen-

tation learning and improve robustness under varying conditions [2, 28], recent works [1, 9] have applied learnable noise to examine adversarial vulnerabilities in VLMs using prompt learning setup. Inspired by this approach, we propose a TTA framework based on noise adaptation.

Our approach, dubbed Test-time Noise Tuning (TNT), relies on *learnable noise*, applied over the augmented views of an input image to enhance regions relevant to its correct classification. The noise is sampled from a standard Gaussian distribution and optimized with a two-fold objective: (1) minimizing marginal entropy [37], an approach that proves effective when applied to input adaptation, as demonstrated previously in label adaptation [27]; and (2) maximizing inter-view consistency, a novel objective introduced to promote consistency across representations of different augmented views of the input image. By ensuring that different augmentations of the image map to similar points in the embedding space, the model learns to focus on core, invariant features over superficial details (see an example in Figure 1.) The learned noise is applied to both the input image and its augmentations in an enhanced inference procedure, with performance further boosted through temperature scaling [20, 31].

In a comparative evaluation against seven strong TTA baselines on two established out-of-distribution benchmarks, our approach proves both more accurate and better calibrated, which is crucial to real-world applications. Our method achieves this performance without considerable latency compared to other methods, and proves highly effective even with a limited parametrization budget. In summary, our main contributions are as follows:

- We propose **TNT**, a novel *noise* adaptation strategy that optimizes VLM’s vision encoder’s input space by incorporating learnable noise at test time for a single test sample, enhancing model robustness to distributional shifts and improving out-of-distribution generalization.
- We introduce an inter-view consistency loss for the noise tuning strategy that minimizes the distance between confident augmented views, fostering more aligned representations and reducing prediction uncertainty. This approach harmonizes the benefits of consistency loss and entropy minimization on top of sole noise adaptation.
- We demonstrate that TNT significantly improves VLM generalization, achieving state-of-the-art performance on a range of natural shift and cross-dataset benchmarks, all with reduced computational overhead.

To the best of our knowledge, we are the first to explore noise optimization for representation learning within VLMs, offering a novel TTA approach. Our findings on TNT highlight the potential of noise-adaptive architectures, encouraging further research into enhancing model robustness and generalization.

2. Related Work

Zero-Shot VLM Generalization: Pre-trained on large image-text datasets in a self-supervised way, VLMs such as CLIP [24] and ALIGN [15] have shown strong generalization capabilities. For example, CLIP’s remarkable zero-shot transfer performance can be attributed to the diversity and scale of the data on which it was trained. Nonetheless, adapting them effectively to specific downstream tasks when data is scarce remains a challenge. One straightforward yet effective approach to enhance CLIP’s zero-shot performance on image classification is the use of *soft prompts* [41] which are *learned* in a few-shot training setup.

Test-Time Optimization: Approaches such as TPT [27] adjust prompts at test time to reduce entropy across augmented views of a single test sample, improving accuracy without additional training data. However, TPT does not address *model calibration*, which is essential for uncertainty estimation. To remedy this, C-TPT [36] improves calibration by optimizing prompt selection based on the dispersion of text features, eliminating the need for labeled data. Reinforcement learning with CLIP feedback (RLCF) [39] further enhances generalization by offering continuous feedback during TTA, correcting predictions and preventing overconfidence associated with entropy minimization in TPT. Sample-wise Temperature Scaling (SaLS) [20] modifies temperature scaling during TTA on top of TPT to boost calibration, refining the model’s confidence. CALIP [8], enhances CLIP’s zero-shot performance by incorporating an attention module that enables interaction between visual and textual features, all without requiring additional training or parameters.

Noise-based Learning: While learnable noise has not been explored for TTA, two recent works – BadCLIP [1] and BAPLE [9] – have used it to inject backdoor triggers into the image encoder’s input within a few-shot training setup. These approaches introduce learnable noise during the prompt learning stage to compromise the VLM, demonstrating that simply adding noise can alter the model’s behavior. This insight raises an intriguing question: *could such noise be harnessed positively?*

3. TNT: Test-Time Noise Tuning

3.1. Zero-shot Image Classification with VLMs

Foundation VLMs, such as CLIP and ALIGN, have been shown to perform well on the task of image classification using a simple but effective zero-shot approach. Given an input image, \mathbf{x} , and a set of class descriptions, $\mathbf{t} = \{t_1, t_2, \dots, t_c\}$ for a total of c classes, the prediction scores can be obtained as:

$$f(\mathbf{x}, \mathbf{t}) = \left\{ \text{sim}(f_I(\mathbf{x}), f_T(t_i)) \right\}_{i=1}^c \quad (1)$$

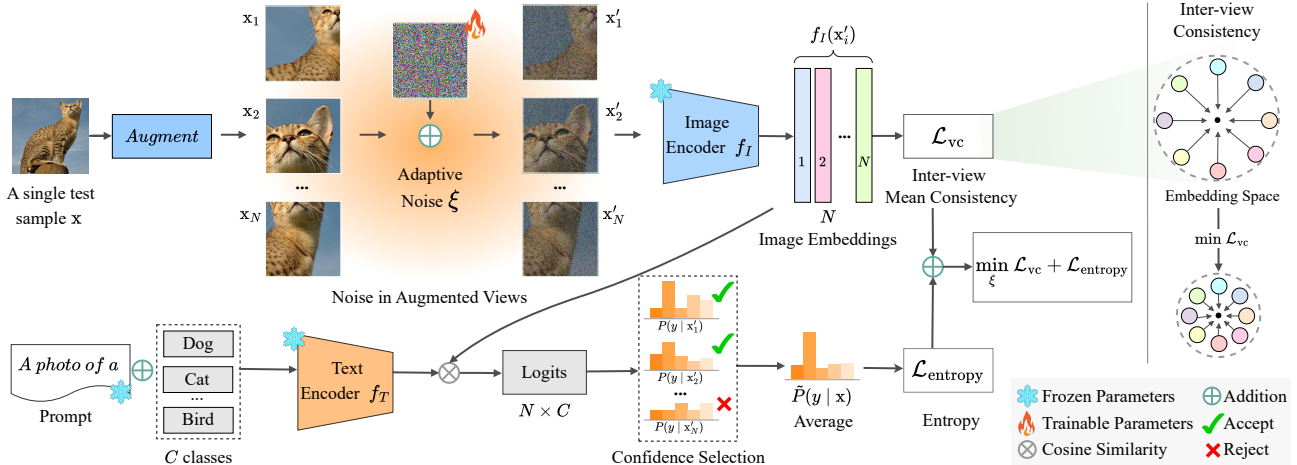


Figure 2. **Test-Time Noise Tuning (TNT)** (1) generates augmented views of a test image, (2) applies adaptive *learnable* noise, and (3) computes logits and feature vectors for each view. (4) Top- K views are selected by confidence, with (5) entropy loss [Eq. 3] enforcing confident predictions and (6) inter-view consistency loss [Eq. 4] aligning feature representations. (7) The combined loss is backpropagated to iteratively refine the noise, enabling adaptive test-time noise tuning.

where f_I denotes the image encoder of the VLM, f_T , the text encoder and $\text{sim}(\cdot)$ is cosine-similarity. For brevity, we hereafter drop \mathbf{t} and denote the scores as $f(\mathbf{x}) \in \mathbb{R}^c$. In this work, we rely on this general framework for zero-shot image classification and experiment specifically with CLIP, without loss of generalization. Although current VLMs exhibit impressive generalization across visual domains and object classes, we aim to improve their performance further through *noise optimization* in the context of TTA.

3.2. Noise Optimization

Unlike traditional fine-tuning, which risks domain-specific biases, prompt tuning refines the input text context to preserve the VLM’s pre-trained features, enhancing its ability to retrieve relevant knowledge with precision. However, relying solely on text optimization may overlook essential visual details. We propose enhancing the image encoder’s input with *learnable* noise, allowing the model to capture subtle features, align with text prompts, and improve performance on varied or noisy images by preserving critical visual cues. Our approach keeps the model’s weights unchanged, preserving its zero-shot capabilities. The workflow of our approach is outlined below.

Noise in Augmented Views: Consider an input image $\mathbf{x} \in \mathbb{R}^{C \times H \times W}$ at test time, where C , H , and W denote channels, height, and width, respectively. To generate diverse views, N *augmented* versions of \mathbf{x} , represented by $(\mathbf{x}_1, \mathbf{x}_2, \dots, \mathbf{x}_N)$, are created using random transformations. The key feature of our approach is a *learnable* noise map $\xi \in \mathbb{R}^{C \times H \times W}$, which is added to each augmented view and tuned through test-time adaptation. Noise values, ξ , are constrained to $[-\epsilon, +\epsilon]$, where ϵ is the perturbation

budget. The perturbed i_{th} augmented view is obtained as follows:

$$\mathbf{x}'_i = \text{clamp}(\mathbf{x}_i + \xi, 0, 1) \quad (2)$$

where $\text{clamp}(\cdot)$ constrains the input values within the valid range $[0, 1]$. At each optimization step, the noise values are iteratively updated to reduce model uncertainty following the objectives described below.

Entropy Loss: The model, $f(\cdot)$, generates logits (unnormalized prediction scores) for each augmented view, denoted as $f(\mathbf{x}'_i)$ for $i \in \{1, 2, \dots, N\}$. Following the approach in [27], we retain only the high-confidence views, selecting the top- K views with lowest self-entropy.¹ Using these top- K views, we compute the marginal entropy loss, denoted by $\mathcal{L}_{\text{entropy}}(\cdot)$, as follows:

$$\mathcal{L}_{\text{entropy}} = \mathcal{H} \left(\frac{1}{K} \sum_{k \in \mathcal{K}} \text{softmax}(f(\mathbf{x}'_k)) \right) \quad (3)$$

where $\mathcal{H}(\cdot)$ computes the entropy of the average probability distribution. This distribution is obtained by first applying $\text{softmax}(\cdot)$ to each logit $f(\mathbf{x}'_k)$ and then averaging the resulting probabilities across the top- K high-confidence views. Here, \mathcal{K} represents the set of indices corresponding to these top- K views.

Inter-view Consistency Loss: To ensure consistency among multiple augmented views, we introduce *inter-view consistency* loss minimization objective to penalize large embedding variations among high-confidence views. Let

¹Notice that the dynamic percentile threshold implemented in [27] effectively implements a top- K selection process as well.

$f_I(\mathbf{x}'_i) \in \mathbb{R}^d$ represent the embedding of perturbed i_{th} augmented view \mathbf{x}'_i . We calculate pairwise Euclidean (ℓ_2) distance among embeddings of the top- K selected views and define the *inter-view consistency* loss, denoted by \mathcal{L}_{vc} , as follows:

$$\mathcal{L}_{\text{vc}} = \sum_{i \in \mathcal{K}} \sum_{j \in \mathcal{K}} \|f_I(\mathbf{x}'_i) - f_I(\mathbf{x}'_j)\|_2 \quad (4)$$

where $i \neq j$. \mathcal{L}_{vc} loss, combined with noise perturbation, penalizes high variance in representations, encouraging the model to maintain stable and consistent feature embeddings for the selected confident views.

Noise Tuning: The final loss \mathcal{L} combines the entropy and inter-view consistency losses i.e. $\mathcal{L} = \alpha \mathcal{L}_{\text{entropy}} + \beta \mathcal{L}_{\text{vc}}$, where α and β control the weights of the respective losses. The learnable noise is adapted by minimizing \mathcal{L} as follows:

$$\underset{\xi}{\text{minimize}} \quad \alpha \mathcal{L}_{\text{entropy}} + \beta \mathcal{L}_{\text{vc}} \quad (5)$$

This objective encourages both high-confidence predictions (through entropy minimization) and consistent embeddings across views (via inter-view distance minimization), thereby enhancing model robustness and calibration under distribution shifts. To update the noise ξ in each iteration, we compute the gradient of the loss \mathcal{L} and update ξ as follows:

$$\xi \leftarrow \xi - \gamma \cdot \text{sign}(\nabla_{\xi} \mathcal{L}) \quad (6)$$

where γ is the learning rate, and $\text{sign}(\cdot)$ denotes the element-wise sign function [7]. After each update step, the noise ξ values are clamped to the interval $[-\epsilon, +\epsilon]$. Algorithm 1 provides a high-level overview of the noise update process in TNT.

Inference: After the noise adaptation phase, during inference, we add the *learned* noise ξ to each of the N augmented views of the image \mathbf{x} . Based on self-entropy, we then select the top- K most confident views, denoted as $\{\mathbf{x}_k + \xi\}_{k \in \mathcal{K}}$. Using Equation 1, we obtain the logits for each of the perturbed top- K views and compute the final probability distribution \mathbf{p} as follows:

$$\mathbf{p} = \frac{1}{K} \sum_{k \in \mathcal{K}} \text{softmax}_{\tau}(f(\mathbf{x}_k + \xi)) \quad (7)$$

where τ is the temperature parameter in the softmax function which scales the obtained logits. The predicted label is then obtained by taking the argmax of the probability distribution i.e.

$$\hat{y} = \underset{i \in \{1, 2, \dots, c\}}{\text{argmax}} \quad p_i \quad (8)$$

where p_i is the probability of i_{th} class in distribution \mathbf{p} .

Algorithm 1 PyTorch style Pseudocode for TNT

```

# image = single test image
# model = pre-trained VLM
# eps = perturbation budget for noise
# lr = learning rate to update noise
# top_k = number of top-K views
# t = number of steps
def TNT(model, image, top_k, t):
    noise = torch.randn(image.shape)
    noise = noise.clamp(-eps, eps)
    # Get N augmented views of test image
    images = augment(image) # (N,C,H,W)
    for step in range(t):
        # Add noise to augmented views of test image
        # and get logits and views' feature vectors
        logits, images_feats = model(images + noise)
        # Get indices of top-K views
        k_indices = confidence_filter(logits, top_k)
        # Compute entropy loss on top-K views
        loss_e = entropy(logits[k_indices])
        # Compute inter-view consistency loss
        loss_vc = vc_loss(images_feats[k_indices])
        loss = loss_e + loss_vc
        loss.backward()
        # Update the learnable noise
        noise = noise - torch.sign(noise.grad) * lr
        noise = noise.clamp(-eps, eps)
    # Inference after noise adaptation
    logits, _ = model(images + noise)
    # Apply temperature scaling on top-K views
    probs = (logits[k_indices]/tau).softmax()
    predicted_label = argmax(probs.mean(dim=0))
    return predicted_label

```

4. Experiments and Results

4.1. Experimental Setup

Datasets: We conduct experiments on a diverse range of benchmark datasets to assess the performance and robustness of our method, specifically testing its out-of-domain generalization across different domains. The selected datasets include ImageNet-A [12], ImageNet-V2 [25], ImageNet-R [11] and ImageNet-Sketch (denoted as ImageNet-K) [33], which have been considered as out-of-distribution (OOD) data for ImageNet to assess model robustness under different conditions and distributions.

For cross-domain generalization, following [27], we include Flowers102 [21], DTD [4], Pets [22], UCF [29], and Caltech101 [5]. These datasets were chosen to analyze the model’s ability to distinguish subtle differences between similar classes. Additionally, we include Aircraft [19], EuroSAT [10], Cars [17], Food [3], and SUN397 [34] to further test the model’s adaptability across distinct categories, including aerial images, satellite images, and object-centric as well as scene-centric datasets.

Implementation Details: We initialize the noise $\xi \in \mathbb{R}^{3 \times 224 \times 224}$ by sampling from a standard Gaussian distri-

Table 1. **Top-1 accuracy** % of state-of-the-art baselines, where **OOD Avg.** indicates the OOD average results and *bs.* indicates the baseline, *i.e.*, CLIP-ViT-B-16. The arrow \blacktriangle and \blacktriangledown indicate **improvements** and **decrements** compared to the CLIP method, *i.e.*, CLIP-ViT-B/16. RLCF* denotes RLCF with all visual encoder parameters trainable. TNT* denotes proposed method with hand crafted prompts while TNT denotes CoOp initialized prompts. **Bold** indicates best performance, Underline indicates second-best.

Method \downarrow	ImageNet	ImageNet-A	ImageNet-V	ImageNet-R	ImageNet-K	Average	OOD Avg.
CLIP-ViT-B/16	67.41(<i>bs.</i>)	47.85(<i>bs.</i>)	60.89(<i>bs.</i>)	73.99(<i>bs.</i>)	46.10(<i>bs.</i>)	59.25(<i>bs.</i>)	57.21(<i>bs.</i>)
CoOp	68.63(1.22) \blacktriangle	50.25(2.40) \blacktriangle	<u>64.95</u> (4.06) \blacktriangle	75.70(1.71) \blacktriangle	48.26(2.16) \blacktriangle	61.56(2.31) \blacktriangle	59.79(2.58) \blacktriangle
TPT _{NIPS '22}	69.86(2.45) \blacktriangle	54.25(6.40) \blacktriangle	63.19(2.30) \blacktriangle	76.90(2.91) \blacktriangle	47.45(1.35) \blacktriangle	62.33(3.08) \blacktriangle	60.45(3.24) \blacktriangle
CALIP _{AAAI '23}	66.74(0.67) \blacktriangledown	47.76(0.09) \blacktriangledown	60.76(0.13) \blacktriangledown	73.99(0.00) \blacktriangledown	46.12(0.02) \blacktriangle	59.07(0.18) \blacktriangledown	57.16(0.05) \blacktriangledown
C-TPT _{ICLR '24}	68.56(1.15) \blacktriangle	50.67(2.82) \blacktriangle	61.56(0.67) \blacktriangle	75.32(1.33) \blacktriangle	46.84(0.74) \blacktriangle	60.59(1.34) \blacktriangle	58.60(1.39) \blacktriangle
SaLS _{ECCV '24}	69.67(2.26) \blacktriangle	54.53(6.68) \blacktriangle	63.22(2.33) \blacktriangle	76.88(2.89) \blacktriangle	47.51(1.41) \blacktriangle	62.36(3.11) \blacktriangle	60.54(3.33) \blacktriangle
RLCF _{ICLR '24}	69.36(1.95) \blacktriangle	54.08(6.23) \blacktriangle	62.71(1.82) \blacktriangle	76.82(2.83) \blacktriangle	47.33(1.23) \blacktriangle	62.06(2.81) \blacktriangle	60.24(3.03) \blacktriangle
RLCF* _{ICLR '24}	70.14(2.73) \blacktriangle	59.24(11.39) \blacktriangle	64.55(3.66) \blacktriangle	<u>77.13</u> (3.14) \blacktriangle	48.50(2.40) \blacktriangle	63.91(4.66) \blacktriangle	62.36(5.15) \blacktriangle
TNT*	<u>70.27</u> (2.86) \blacktriangle	<u>61.87</u> (14.02) \blacktriangle	63.64(2.75) \blacktriangle	76.96(2.97) \blacktriangle	48.03(1.93) \blacktriangle	<u>64.15</u> (4.90) \blacktriangle	<u>62.63</u> (5.42) \blacktriangle
TNT	72.06 (4.65) \blacktriangle	63.93 (16.08) \blacktriangle	66.64 (5.75) \blacktriangle	78.61 (4.62) \blacktriangle	49.16 (3.06) \blacktriangle	66.08 (6.83) \blacktriangle	64.59 (7.38) \blacktriangle

bution and set $\epsilon = 1/255$. This noise is applied to $N = 64$ images, consisting of the original image and 63 augmented views, which are generated through random resized crops and horizontal flips of the original image. Noise is updated with a learning rate of $1e-3$ across all datasets. For temperature scaling, we use a constant value of $\tau = 7e-3$ across all settings. We use fixed prompts in two configurations: first, a hand-crafted prompt (“a photo of a {CLASS}”), referred to as TNT*; and second, 4-shot context weights obtained using CoOp [41] on ImageNet, referred to as TNT. All experiments are conducted on a single NVIDIA A6000 48GB GPU.

Baselines: We evaluate a total of seven zero-shot baselines to assess the effectiveness of our approach. In addition to CLIP zero-shot [24] and CLIP with the CoOp pretrained soft prompt [42], we *reproduce* several recently published test-time adaptation methods: TPT [27], CALIP [8], C-TPT [36], SaLS [20] and RLCF [40]. All methods are reproduced on our system with a single update step and the same consistent backbones to ensure fair comparisons. Specifically, we use the same backbone for both the teacher and student models in RLCF.

4.2. TNT Results

Natural Distribution Shifts: Table 1 compares our method with seven baselines using a ViT-B/16 backbone, including zero-shot CLIP. Our simpler variant, TNT*, which uses a hand-crafted prompt, achieves the highest average performance across four OOD datasets and in-domain on ImageNet. This demonstrates that adapting input features through noise learning with marginal entropy and inter-view distance minimization effectively enhances classification accuracy. We achieve this *without having to modify the large vision encoder* itself, as was done in RLCF*, yet we score substantially higher at a lower computational cost. While TNT* shows a minor in-domain improvement over TPT (< 0.5 points), it achieves a substantial OOD gain

(around 2 points), with ImageNet-A benefiting notably from noise adaptation. Further analysis of trainable parameters and text vs. image adaptation is detailed in §5.1.

Our stronger variant, TNT, uses a CoOp-initialized prompt in the text encoder, yielding an additional 2 points in average performance both in- and out-of-domain. Interestingly, CoOp alone ranks poorly among the baselines, underperforming TNT by nearly 5 points. We observe an interesting synergy where the CoOp in itself has limited capacity but proves very effective as an initialization technique in TNT, enabling noise to adapt visual features and improving classification performance. In §5.2, we show that further tuning this prompt calibrates model predictions but does not improve accuracy.

Cross-Dataset Generalization: Table 2 shows TNT’s cross-dataset evaluation across ten datasets, following [27]. TNT outperforms all baselines with an average accuracy of 64.48% and achieving top generalization on seven out of ten datasets. TNT* also performs well, averaging 64.07% and surpassing CLIP, CoOp, and TPT on several datasets. Notably, TNT* excels over TPT on OxfordPets, UCF, Aircraft, and StanfordCars. TNT’s use of learnable noise enhances the visual feature space, capturing subtle distinctions across datasets and ensuring consistent, class-specific embeddings for improved zero-shot generalization, all without modifying the pre-trained model. The minimization of inter-view mean distance ensures consistent embeddings, enhancing the model’s ability to differentiate class-specific details that TPT [27] and RLCF [39] miss.

5. Analysis and Ablations

We conduct extensive analysis and ablations to assess how design choices impact performance, using the ImageNet-A benchmark with the ViT-B/16 backbone for consistency, as it represents a basic domain generalization variant.

Table 2. **Top-1 accuracy** % of state-of-the-art baselines, where **Average** indicates average accuracies of the *Cross-Datasets Generalization*. The arrow \blacktriangle and \blacktriangledown indicate **improvements** and **decrements** compared to the CLIP-ViT-B/16. TNT* denotes the proposed method with hand-crafted prompts while TNT denotes CoOp initialized prompts. **Bold** indicates best performance, Underline indicates second-best.

Method \downarrow	Flower102[21]	DTD[4]	OxfordPets[22]	UCF[29]	Caltech101[5]	Aircraft[19]
CLIP-ViT-B/16	67.92(<i>bs.</i>)	44.27(<i>bs.</i>)	88.28(<i>bs.</i>)	65.21(<i>bs.</i>)	93.39(<i>bs.</i>)	23.82(<i>bs.</i>)
CoOp	<u>68.82</u> (0.90) \blacktriangle	39.24(5.03) \blacktriangledown	<u>89.53</u> (1.25) \blacktriangle	<u>68.51</u> (3.30) \blacktriangle	90.71(2.68) \blacktriangledown	20.01(3.81) \blacktriangledown
TPT _{NIPS '22}	68.58(0.66) \blacktriangle	45.27 (1.00) \blacktriangle	86.29(2.00) \blacktriangledown	67.62(2.41) \blacktriangle	93.35(0.04) \blacktriangledown	22.02(1.80) \blacktriangledown
CALIP _{AAAI '23}	67.64(0.28) \blacktriangledown	44.44(0.17) \blacktriangle	87.82(0.46) \blacktriangledown	64.05(1.16) \blacktriangledown	93.27(0.12) \blacktriangledown	<u>24.12</u> (0.30) \blacktriangle
C-TPT _{ICLR '24}	70.24 (2.32) \blacktriangle	44.74(0.47) \blacktriangle	87.73(0.55) \blacktriangledown	64.37(0.84) \blacktriangledown	92.41(0.98) \blacktriangledown	23.76(0.06) \blacktriangledown
SaLS _{ECCV '24}	68.66(0.74) \blacktriangle	<u>45.15</u> (0.88) \blacktriangle	86.40(1.88) \blacktriangledown	67.38(2.17) \blacktriangle	93.51(0.12) \blacktriangle	21.93(1.89) \blacktriangledown
RLCF _{ICLR '24}	68.13(0.21) \blacktriangle	45.15(0.88) \blacktriangle	86.56(1.72) \blacktriangledown	66.96(1.75) \blacktriangle	<u>94.04</u> (0.65) \blacktriangle	21.51(2.31) \blacktriangledown
TNT*	66.26(1.66) \blacktriangledown	43.85(0.42) \blacktriangledown	87.84(0.44) \blacktriangledown	67.89(2.68) \blacktriangle	93.31(0.08) \blacktriangledown	24.54 (0.72) \blacktriangle
TNT	68.74(0.82) \blacktriangle	41.71(2.56) \blacktriangledown	89.59 (1.31) \blacktriangle	68.81 (3.60) \blacktriangle	94.66 (1.27) \blacktriangle	20.65(3.17) \blacktriangledown

Method \downarrow	EuroSAT[10]	StanfordCars[17]	Food101[3]	SUN397[34]	Average
CLIP-ViT-B/16	42.02(<i>bs.</i>)	65.59(<i>bs.</i>)	83.65(<i>bs.</i>)	62.61(<i>bs.</i>)	63.68(<i>bs.</i>)
CoOp	41.78(0.24) \blacktriangledown	64.74(0.85) \blacktriangledown	83.96(0.31) \blacktriangle	64.67(2.06) \blacktriangle	63.20(0.48) \blacktriangledown
TPT _{NIPS '22}	42.81(0.79) \blacktriangle	66.57(0.98) \blacktriangle	<u>84.47</u> (0.82) \blacktriangle	<u>64.82</u> (2.21) \blacktriangle	64.18(0.50) \blacktriangle
CALIP _{AAAI '23}	42.27(0.25) \blacktriangle	66.50(0.91) \blacktriangle	86.93 (3.28) \blacktriangle	63.48(0.87) \blacktriangle	64.05(0.37) \blacktriangle
C-TPT _{ICLR '24}	36.33(5.69) \blacktriangledown	64.77(0.82) \blacktriangledown	81.67(2.98) \blacktriangledown	62.56(0.05) \blacktriangledown	62.86(0.82) \blacktriangledown
SaLS _{ECCV '24}	42.53(0.51) \blacktriangle	66.73(1.14) \blacktriangle	84.47(0.82) \blacktriangle	64.81(2.20) \blacktriangle	64.16(0.48) \blacktriangle
RLCF _{ICLR '24}	45.28 (3.26) \blacktriangle	65.85(0.26) \blacktriangle	84.06(0.41) \blacktriangle	64.59(1.98) \blacktriangle	<u>64.21</u> (0.53) \blacktriangle
TNT*	41.99(0.03) \blacktriangledown	<u>66.93</u> (1.34) \blacktriangle	84.10(0.45) \blacktriangle	64.03(1.42) \blacktriangle	64.07(0.39) \blacktriangle
TNT	<u>44.31</u> (2.29) \blacktriangle	67.38 (1.79) \blacktriangle	83.94(0.29) \blacktriangle	65.00 (2.39) \blacktriangle	64.48 (0.80) \blacktriangle

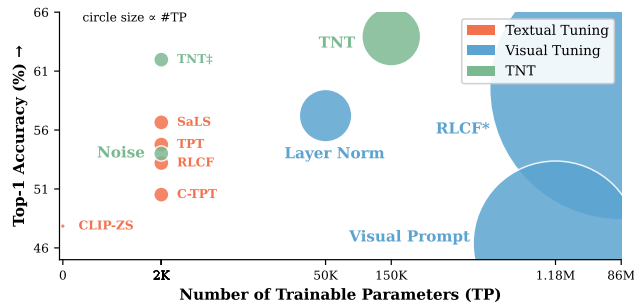


Figure 3. **Analysis of Trainable Parameters (TP)** for TNT, textual tuning, and encoder tuning. Circle size indicates the #TP. **Textual Tuning** methods use the same TP count of 2K to optimize prompts. **RLCF*** refers to RLCF with all visual encoder parameters trainable, **Layer Norm** limits trainable parameters of visual encoder to only Layer Norms, and **Visual Prompt** applies learnable prompts to the visual encoder across 12 layers of the ViT encoder. **TNT \ddagger** indicates TNT with only 224×9 trainable noise parameters, compared to standard TNT with $224 \times 224 \times 3$ TP. **Noise** denotes optimization with 224×9 TP in noise and with only $\mathcal{L}_{\text{entropy}}$ loss.

5.1. Computational Analysis

Trainable Parameters (TP) vs. Accuracy: Test-time tuning methods like TPT, C-TPT, SaLS, and RLCF (prompt-tuning variant) adapt textual prompts with only 2048 TP (4 tokens of $d=512$) but show limited generalization, with Top-1 ImageNet-A accuracy around 50% to 55%. In contrast, visual adaptation based methods *e.g.* encoder tuning, visual prompting, and layer norm optimization—require more TP.

As depicted in Figure 3, these Visual Tuning approaches offer moderate to lower generalization with increased TP, and that too while accessing the encoder itself. In contrast, TNT effectively balances this trade-off with 150k ($224 \times 224 \times 3$) TP, achieving the highest generalization at 63.93, *while preserving the black-box assumption*. Remarkably in our ablation, when TNT is initialized with 2016 (224×9) TP (similar to the parameter count of textual tuning methods), it still demonstrates stronger generalization than baselines, highlighting its adaptability in handling distribution shifts through noise tuning. Furthermore, when TNT’s noise component (with 2016 TP) is tuned using only entropy (without \mathcal{L}_{vc} or temperature-scaled inference), it achieves performance on par with that of textual tuning approaches.

Trade-off between Accuracy, Time, and Memory: Table 3 shows that TNT achieves the highest performance while maintaining optimal inference time and memory efficiency if not the best. Although TNT demands a moderate memory increase (8.57 GB), it maintains practical inference speed and accuracy compared to alternatives like C-TPT, which incurs higher memory (up to 33.44 GB for ImageNet-V) and slower inference times. However, our approach demonstrates the best trade-off by achieving top accuracy with efficient memory use, especially in cases where feature complexity necessitates higher resource allocation for robust predictions.

Table 3. Average GPU inference time per sample and memory usage across different optimization steps. Top-1 Accuracy (Acc), inference time in seconds (Time), and memory usage in GB (Mem) are shown for each method. **Bold** indicates best performance.

Method ↓	Steps	ImageNet-A			ImageNet-V		
		Acc	Time	Mem	Acc	Time	Mem
CLIP-ViT-B/16	0	47.85	0.05	2.06	60.89	0.20	3.73
TPT _{NIPS '22}	1	54.31	0.21	5.05	63.19	0.71	18.35
	3	57.91	0.50	5.05	65.02	1.76	18.35
C-TPT _{ICLR '24}	1	50.52	0.36	8.19	61.56	1.23	33.44
	3	54.42	0.96	8.19	64.72	3.32	33.44
SaLS _{ECCV '24}	1	56.65	0.21	5.05	63.22	0.71	18.35
	3	58.16	0.51	5.05	64.57	1.76	18.35
RLCF _{ICLR '24}	1	54.77	0.22	5.05	62.71	0.73	18.35
	3	57.27	0.52	5.05	64.02	1.78	18.35
TNT	1	63.93	0.33	8.57	66.64	0.87	21.89
	3	65.17	0.79	8.57	67.10	2.09	21.89

5.2. Ablations

Effect of Different Components: Although TNT’s noise tuning shows enhanced results, it is intriguing to understand how each component contributes to improved generalization and calibration. As depicted in Figure 4, initialized noise, when optimized with only entropy (**E**), shows comparable generalization and calibration to textual tuning baselines. Adding the inter-view consistency loss (**E+V**) improves the alignment of image embeddings, resulting in more consistent and confident predictions. This approach not only outperforms entropy minimization alone but also reduces the Expected Calibration (EC) error by 3%. Intuitively, this process encourages the embeddings to be closer in feature space, leading to lower intra-class variance while preserving inter-class differences. Furthermore, during inference, applying temperature τ to scale the output logits (Eq. 7), as in **E+V+T'**, increases accuracy by 3%. Extending this approach to consider the top- K views, as in **E+V+T**, further improves performance by 2%. This configuration corresponds to our TNT* variant. The top- K strategy focuses final predictions on the most confident views rather than relying solely on a single sample, resulting in notable accuracy gains. When TNT* is initialized with CoOp, resulting in **TNT**, it achieves the highest generalization (63.93 Top-1 accuracy) and reliable calibration error [20, 36]. TNT achieves an ECE of 11.46, second only to C-TPT, while outperforming all other baselines in accuracy. This result indicates strong uncertainty estimation with effective noise tuning.

Impact of Combinative Tuning: Assumably, when combining the proposed TNT with prompt tuning (PT) or encoder tuning (ET), one might expect better generalization. Interestingly, we observe in Figure 4 that both **TNT+PT**

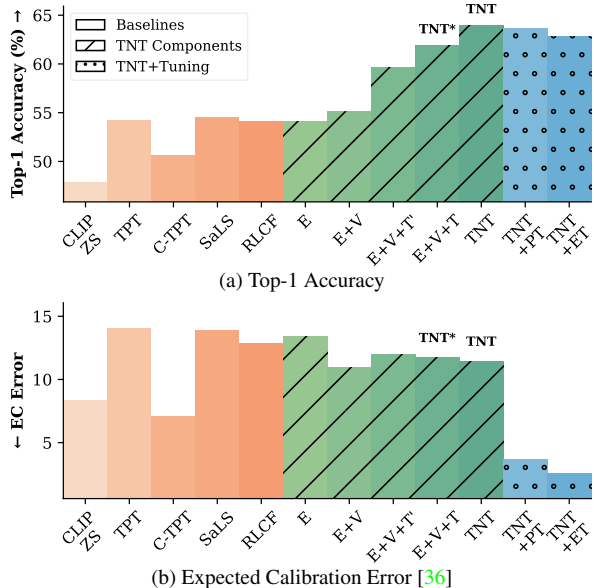


Figure 4. Effect of TNT Components on (a) Top-1 Accuracy (Higher \uparrow is better) and (b) ECE (Lower \downarrow is better). **E**: Noise optimization with Entropy minimization $\mathcal{L}_{\text{entropy}}$. **E+V**: Adds \mathcal{L}_{vc} loss (Eq. 4) to $\mathcal{L}_{\text{entropy}}$. **E+V+T'**: Adds temperature scaling during inference to E+V. **E+V+T**: Makes use of top- K views instead of one test image (Eq. 7), i.e. TNT*. **TNT**: TNT* with CoOp initialization, **TNT+PT** (Prompt Tuning): Optimizes textual prompts with TNT. **TNT+ET** (Encoder Tuning): Optimizes the visual encoder with TNT. Optimization Steps $t = 1$ is used consistently. The same Legend is used for (a) and (b).

and **TNT+ET** achieve comparable generalization to TNT while significantly improving calibration error. Intuitively, this is because **TNT+PT** refines the alignment between textual and visual features, enhancing calibration. On the other hand, **TNT+ET** improves calibration by allowing the model to better align its learned visual representations with the specific distribution of the input data. This shows that calibration error can be further minimized by optimizing the interaction between the model’s visual and textual components, on top of the TNT framework.

Effect of Optimization Steps: All reported results thus far have been obtained with a single training step; however, we observe that TNT’s efficacy is influenced by the number of optimization steps, impacting both accuracy and ECE [36]. In Figure 5(a)(left), we observe that increasing the number of steps leads to a 2% performance gain for both TNT* and TNT configurations from step $t = 1$ to $t = 5$. While other baselines follow a similar trend across optimization steps, they exhibit lower accuracy compared to TNT, indicating TNT’s adaptability for more efficient applications. Interestingly, in Figure 5(a)(right), we find that TNT variants achieve notably lower calibration error with more optimization steps, as TNT* reaches an ECE of 5.67 at step $t = 5$, outperforming zero-shot CLIP (ECE 8.32) and other base-

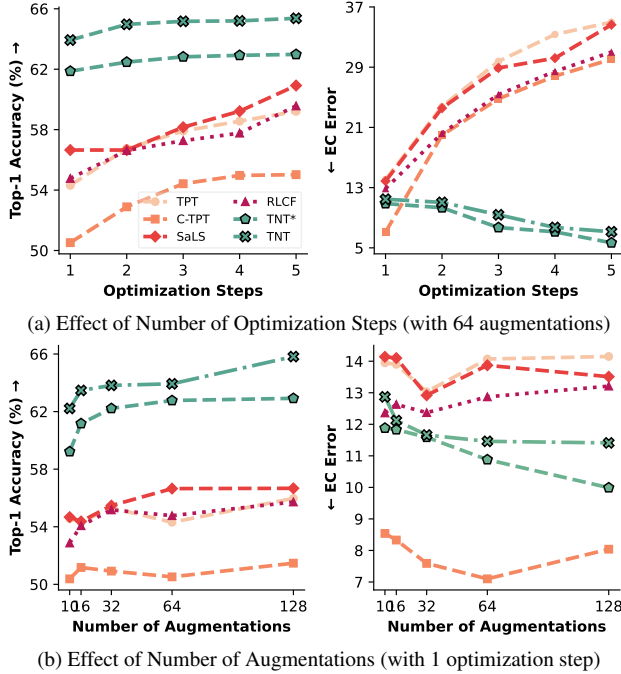


Figure 5. Increasing the number of optimization steps and augmentations both result in higher (a) **Top-1 Accuracy**, and lower (b) **Expected Calibration (EC) Error**. TNT* and TNT denote hand-crafted and CoOp-based prompts, respectively. The legend is shared throughout.

lines by a considerable margin. The additional optimization steps in TNT encourage the noise to increasingly adapt to more representative features, as shown in Figure 1.

Effect of Number of Augmentations: Similarly, accuracy improves with an increasing number of augmentations across TNT configurations and baselines, reaching a plateau at $N = 64$ for most baselines as shown in Figure 5(b)(left). Notably, TNT achieves a Top-1 Accuracy of 65.82 with 128 augmentations, though with higher memory requirements. In contrast, TNT* sees a modest 0.20% increase from $N = 64$ to $N = 128$ augmentations. Regarding ECE, TNT also reduces ECE with an increasing number of augmentation steps, where TNT* achieves the second-best ECE at 9.99, following C-TPT at 8.04, while TPT reaches 14.15 as shown in Figure 5(b)(right). Varied augmentations provide more *diverse* and class-specific crops, leading to better overall generalization and lower EC error. Given the linear increase in memory usage associated with additional augmentations, we adopt single-step optimization as the default setting for both TNT* and TNT, as they already improve the average OOD accuracy over zero-shot CLIP by 5.42% and 7.38% respectively.

5.3. Qualitative Analysis

Impact of Noise Optimization on Attention Maps: TNT optimizes noise in a way that it *implicitly* influences the in-

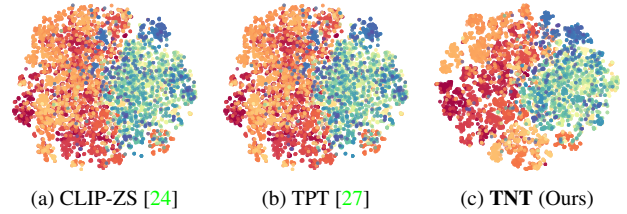


Figure 6. **t-SNE visualizations** of the final class embedding from the test sets of ImageNet-A dataset, following Table 1. TNT could produce *more clustered and separable features* than other zero-shot generalization baselines.

put’s attention maps, guiding the model to adaptively focus on the most relevant features within the test input. This process enables TNT to dynamically emphasize important regions, ensuring the model attends to critical information for each sample. As illustrated in Figure 1, there is a noticeable refinement in the attention between the original and adapted samples; with each optimization step, the adapted noise becomes increasingly *aligned* with the salient features, effectively suppressing irrelevant details and amplifying relevant cues. This progressive adaptation results in more confident and accurate predictions, as the model’s focus narrows on features that are contextually meaningful and better aligned with the target task.

Feature Shifts via Adaptation: Figure 6 examines the shift in the distribution of visual features after optimization, comparing the results from baselines and TNT. As depicted, CLIP-ZS and TPT show scattered feature distributions, reflecting their struggle to distinguish class boundaries effectively in naturally shifted data. In contrast, TNT demonstrates tightly *clustered* and *well-separated* features, which suggests that TNT’s noise adaptation mechanism and consistency losses promote feature alignment and separation more effectively than entropy-based or prompt-tuning methods alone. This focused feature adaptation helps establish more *defined decision boundaries* and mitigates the impact of irrelevant features, thus leading to better overall performance on out-of-distribution samples.

6. Conclusion

We introduce Test-Time Noise Tuning (TNT), a novel noise adaptation strategy for zero-shot settings that enhances out-of-distribution generalization by tuning a learnable noise for visual input of a VLM, improving robustness and calibration. TNT demonstrates the potential of noise tuning in challenging VLM benchmarks, setting a foundation for adaptive OOD handling. Our noise tuning demonstrates, for the first time, a positive impact on representation learning in VLMs, paving the way for further exploration across other modalities. Extending TNT’s noise tuning and inter-view consistency loss to other vision-language tasks, such as re-

trieval, as well as applications like medical imaging, would be valuable. A promising direction for future research is to explore strategies for reducing the memory requirements of TNT, enhancing its scalability and applicability in resource-constrained environments.

References

- [1] Jiawang Bai, Kuofeng Gao, Shaobo Min, Shu-Tao Xia, Zhifeng Li, and Wei Liu. Badclip: Trigger-aware prompt learning for backdoor attacks on clip. In *Proceedings of the IEEE/CVF Conference on Computer Vision and Pattern Recognition*, pages 24239–24250, 2024. 2
- [2] Yoshua Bengio, Aaron Courville, and Pascal Vincent. Representation learning: A review and new perspectives. *IEEE Transactions on Pattern Analysis and Machine Intelligence*, 35(8):1798–1828, 2013. 2
- [3] Lukas Bossard, Matthieu Guillaumin, and Luc Van Gool. Food-101—mining discriminative components with random forests. In *Computer vision—ECCV 2014: 13th European conference, zurich, Switzerland, September 6–12, 2014, proceedings, part VI 13*, pages 446–461. Springer, 2014. 4, 6
- [4] Mircea Cimpoi, Subhansu Maji, Iasonas Kokkinos, Sammy Mohamed, and Andrea Vedaldi. Describing textures in the wild. In *Proceedings of the IEEE conference on computer vision and pattern recognition*, pages 3606–3613, 2014. 4, 6
- [5] Li Fei-Fei, Rob Fergus, and Pietro Perona. Learning generative visual models from few training examples: An incremental bayesian approach tested on 101 object categories. In *2004 conference on computer vision and pattern recognition workshop*, pages 178–178. IEEE, 2004. 4, 6
- [6] Ian Goodfellow, Jean Pouget-Abadie, Mehdi Mirza, Bing Xu, David Warde-Farley, Sherjil Ozair, Aaron Courville, and Yoshua Bengio. Generative adversarial nets. *Advances in neural information processing systems*, 27, 2014. 1
- [7] Ian J. Goodfellow, Jonathon Shlens, and Christian Szegedy. Explaining and harnessing adversarial examples, 2015. 4
- [8] Ziyu Guo, Renrui Zhang, Longtian Qiu, Xianzheng Ma, Xupeng Miao, Xuming He, and Bin Cui. Calip: Zero-shot enhancement of clip with parameter-free attention. In *Proceedings of the AAAI Conference on Artificial Intelligence*, pages 746–754, 2023. 2, 5
- [9] Asif Hanif, Fahad Shamshad, Muhammad Awais, Muazzam Naseer, Fahad Shahbaz Khan, Karthik Nandakumar, Salman Khan, and Rao Muhammad Anwer. Baple: Backdoor attacks on medical foundational models using prompt learning. In *International Conference on Medical Image Computing and Computer-Assisted Intervention*, pages 443–453. Springer, 2024. 2
- [10] Patrick Helber, Benjamin Bischke, Andreas Dengel, and Damian Borth. Eurosat: A novel dataset and deep learning benchmark for land use and land cover classification. *IEEE Journal of Selected Topics in Applied Earth Observations and Remote Sensing*, 12(7):2217–2226, 2019. 4, 6
- [11] Dan Hendrycks, Steven Basart, Norman Mu, Saurav Kadavath, Frank Wang, Evan Dorundo, Rahul Desai, Tyler Zhu, Samyak Parajuli, Mike Guo, et al. The many faces of robustness: A critical analysis of out-of-distribution generalization. In *Proceedings of the IEEE/CVF international conference on computer vision*, pages 8340–8349, 2021. 4
- [12] Dan Hendrycks, Kevin Zhao, Steven Basart, Jacob Steinhardt, and Dawn Song. Natural adversarial examples. In *Proceedings of the IEEE/CVF conference on computer vision and pattern recognition*, pages 15262–15271, 2021. 4
- [13] Jonathan Ho, Ajay Jain, and Pieter Abbeel. Denoising diffusion probabilistic models. *Advances in neural information processing systems*, 33:6840–6851, 2020. 1
- [14] Raza Imam, Hanan Gani, Muhammad Huzaifa, and Karthik Nandakumar. Test-time low rank adaptation via confidence maximization for zero-shot generalization of vision-language models, 2024. 1
- [15] Chao Jia, Yinfei Yang, Ye Xia, Yi-Ting Chen, Zarana Parekh, Hieu Pham, Quoc Le, Yun-Hsuan Sung, Zhen Li, and Tom Duerig. Scaling up visual and vision-language representation learning with noisy text supervision. In *International conference on machine learning*, pages 4904–4916. PMLR, 2021. 2
- [16] Diederik P Kingma. Auto-encoding variational bayes. *arXiv preprint arXiv:1312.6114*, 2013. 1
- [17] Jonathan Krause, Michael Stark, Jia Deng, and Li Fei-Fei. 3d object representations for fine-grained categorization. In *Proceedings of the IEEE international conference on computer vision workshops*, pages 554–561, 2013. 4, 6
- [18] Yanghao Li, Naiyan Wang, Jianping Shi, Jiaying Liu, and Xiaodi Hou. Revisiting batch normalization for practical domain adaptation, 2016. 1
- [19] Subhansu Maji, Esa Rahtu, Juho Kannala, Matthew Blaschko, and Andrea Vedaldi. Fine-grained visual classification of aircraft. *arXiv preprint arXiv:1306.5151*, 2013. 4, 6
- [20] Balamurali Murugesan, Julio Silva-Rodriguez, Ismail Ben Ayed, and Jose Dolz. Robust calibration of large vision-language adapters. *arXiv preprint arXiv:2407.13588*, 2024. 1, 2, 5, 7
- [21] Maria-Elena Nilsback and Andrew Zisserman. Automated flower classification over a large number of classes. In *2008 Sixth Indian conference on computer vision, graphics & image processing*, pages 722–729. IEEE, 2008. 4, 6
- [22] Omkar M Parkhi, Andrea Vedaldi, Andrew Zisserman, and CV Jawahar. Cats and dogs. In *2012 IEEE conference on computer vision and pattern recognition*, pages 3498–3505. IEEE, 2012. 4, 6
- [23] Alec Radford. Unsupervised representation learning with deep convolutional generative adversarial networks. *arXiv preprint arXiv:1511.06434*, 2015. 1
- [24] Alec Radford, Jong Wook Kim, Chris Hallacy, Aditya Ramesh, Gabriel Goh, Sandhini Agarwal, Girish Sastry, Amanda Askell, Pamela Mishkin, Jack Clark, et al. Learning transferable visual models from natural language supervision. In *International conference on machine learning*, pages 8748–8763. PMLR, 2021. 2, 5, 8
- [25] Benjamin Recht, Rebecca Roelofs, Ludwig Schmidt, and Vaishaal Shankar. Do imagenet classifiers generalize to imagenet? In *International conference on machine learning*, pages 5389–5400. PMLR, 2019. 4

- [26] Danilo Jimenez Rezende, Shakir Mohamed, and Daan Wierstra. Stochastic backpropagation and approximate inference in deep generative models. In *International conference on machine learning*, pages 1278–1286. PMLR, 2014. [1](#)
- [27] Manli Shu, Weili Nie, De-An Huang, Zhiding Yu, Tom Goldstein, Anima Anandkumar, and Chaowei Xiao. Test-time prompt tuning for zero-shot generalization in vision-language models. *Advances in Neural Information Processing Systems*, 35:14274–14289, 2022. [1](#), [2](#), [3](#), [4](#), [5](#), [8](#)
- [28] Yang Song, Jascha Sohl-Dickstein, Diederik P Kingma, Abhishek Kumar, Stefano Ermon, and Ben Poole. Generative modeling by estimating gradients of the data distribution. In *Advances in Neural Information Processing Systems*, pages 11918–11930, 2019. [2](#)
- [29] K Soomro. Ucf101: A dataset of 101 human actions classes from videos in the wild. *arXiv preprint arXiv:1212.0402*, 2012. [4](#), [6](#)
- [30] Yu Sun, Xiaolong Wang, Zhuang Liu, John Miller, Alexei Efros, and Moritz Hardt. Test-time training with self-supervision for generalization under distribution shifts. In *International conference on machine learning*, pages 9229–9248. PMLR, 2020. [1](#)
- [31] Weijie Tu, Weijian Deng, Dylan Campbell, Stephen Gould, and Tom Gedeon. An empirical study into what matters for calibrating vision-language models. *arXiv preprint arXiv:2402.07417*, 2024. [2](#)
- [32] Dequan Wang, Evan Shelhamer, Shaoteng Liu, Bruno Olshausen, and Trevor Darrell. Tent: Fully test-time adaptation by entropy minimization. *arXiv preprint arXiv:2006.10726*, 2020. [1](#)
- [33] Haohan Wang, Songwei Ge, Zachary Lipton, and Eric P Xing. Learning robust global representations by penalizing local predictive power. *Advances in Neural Information Processing Systems*, 32, 2019. [4](#)
- [34] Jianxiong Xiao, James Hays, Krista A Ehinger, Aude Oliva, and Antonio Torralba. Sun database: Large-scale scene recognition from abbey to zoo. In *2010 IEEE computer society conference on computer vision and pattern recognition*, pages 3485–3492. IEEE, 2010. [4](#), [6](#)
- [35] Zehao Xiao and Cees GM Snoek. Beyond model adaptation at test time: A survey. *arXiv preprint arXiv:2411.03687*, 2024. [1](#)
- [36] Hee Suk Yoon, Eunseop Yoon, Joshua Tian Jin Tee, Mark A Hasegawa-Johnson, Yingzhen Li, and Chang D Yoo. C-tpt: Calibrated test-time prompt tuning for vision-language models via text feature dispersion. In *The Twelfth International Conference on Learning Representations*. [1](#), [2](#), [5](#), [7](#)
- [37] Marvin Zhang, Sergey Levine, and Chelsea Finn. Memo: Test time robustness via adaptation and augmentation. *Advances in neural information processing systems*, 35:38629–38642, 2022. [2](#)
- [38] Marvin Zhang, Sergey Levine, and Chelsea Finn. Memo: Test time robustness via adaptation and augmentation, 2022. [1](#)
- [39] Shuai Zhao, Xiaohan Wang, Linchao Zhu, and Yi Yang. Test-time adaptation with clip reward for zero-shot generalization in vision-language models. In *The Twelfth International Conference on Learning Representations*. [2](#), [5](#)
- [40] Shuai Zhao, Xiaohan Wang, Linchao Zhu, and Yi Yang. Test-time adaptation with clip reward for zero-shot generalization in vision-language models. *arXiv preprint arXiv:2305.18010*, 2023. [1](#), [5](#)
- [41] Kaiyang Zhou, Jingkang Yang, Chen Change Loy, and Ziwei Liu. Learning to prompt for vision-language models. *International Journal of Computer Vision (IJCV)*, 2022. [2](#), [5](#)
- [42] Kaiyang Zhou, Jingkang Yang, Chen Change Loy, and Ziwei Liu. Learning to prompt for vision-language models. *International Journal of Computer Vision*, 130(9):2337–2348, 2022. [5](#)